

Nanoscale

Accepted Manuscript



This is an *Accepted Manuscript*, which has been through the Royal Society of Chemistry peer review process and has been accepted for publication.

Accepted Manuscripts are published online shortly after acceptance, before technical editing, formatting and proof reading. Using this free service, authors can make their results available to the community, in citable form, before we publish the edited article. We will replace this *Accepted Manuscript* with the edited and formatted *Advance Article* as soon as it is available.

You can find more information about *Accepted Manuscripts* in the [Information for Authors](#).

Please note that technical editing may introduce minor changes to the text and/or graphics, which may alter content. The journal's standard [Terms & Conditions](#) and the [Ethical guidelines](#) still apply. In no event shall the Royal Society of Chemistry be held responsible for any errors or omissions in this *Accepted Manuscript* or any consequences arising from the use of any information it contains.



Nanoscale

ARTICLE

Thermoplasmonic effect of silver nanoparticles modulates peptide amphiphile fiber into nanowreath like assembly[†]

Narendra Kumar Mishra,^{#, a} Vikas Kumar,^{#, b} and Khashti Ballabh Joshi^{*b}

Received 00th January 20xx,
Accepted 00th January 20xx

DOI: 10.1039/x0xx00000x

www.rsc.org/

This study demonstrates the beneficial role of di-tryptophan containing short peptide amphiphiles (sPA) for the synthesis and stabilization of AgNPs in the presence of sunlight followed by garlanding of AgNPs along the fibrous network of sPA. Such hybrid structures were precisely and selectively moulded into Nanowreath kind of morphology due to thermoplasmonic effect of AgNPs and can be used for the several bio-nanotechnological applications.

Biomolecule assisted synthesis of novel nanoparticles and their organization highly depends upon the specific functional group.¹⁻³ These functional groups are responsible to nucleate and to help in the directional growth of nanoparticles and also to facilitate the organization of presynthesized nanomaterials.⁴⁻⁶ The specific functional group present on biological building blocks such as peptides and proteins, promotes and helps to precise and localized deposition of the selective metal (ions) nanoparticles upon the desired supramolecular architectures.⁷⁻¹² Innovative bio-derived nanomaterials have received tremendous attention owing to their optoelectronic or thermoplasmonic properties¹³⁻²⁰ and showed diverse applications from biotechnology to optoelectronics.^{21,22} Fabrications of numerous nanostructures from peptide and peptide based conjugates are essential due to their ease of synthesis, biocompatibility, specific molecular recognition and simple chemical and biological modifications.²³⁻²⁸ Different class of peptides viz; amphiphilic, aromatic rich and surfactant have already been used for nanofabrication and showed exciting potential applications for nanotechnology.²⁹⁻³³ Unique and special features of amphiphilic peptides provide flexible templates for metal nanomaterials and therefore potential biological candidate for the growth and constructing metal based fascinating hybrid nanostructures.³⁴⁻³⁷

Peptides containing aromatic amino acids and their conjugates are well known to self-assemble into distinct and ordered structures and can be used for medical, biomedical and nanosciences applications.³⁸⁻⁴⁰ Tryptophan is the only one aromatic amino acid other than tyrosine that have unique photophysical and photochemical properties therefore tryptophan containing

conjugates are primarily used by researcher as an efficient probes to unravel biotechnological problems.³⁹ Alternatively engineering various classes of nanomaterials with the help of tryptophan rich aromatic conjugates have now become very dynamic, emergent and interested area of research in nanotechnology too.⁴⁰⁻⁴⁵ Tryptophan based short peptide amphiphiles, a special class of peptide conjugates, can also be exploited for the formation of biologically active metal-hybrid nanostructures.^{46,47} Literature reported that defined nanostructures of tryptophan-based peptide amphiphiles can simply be modulated by changing the physical and chemical parameters. These nanostructures were further used as a template for the fabrication and encapsulation of metal nanoparticles, primarily gold and silver nanoparticles.⁴⁷ The gold and silver nanoparticles were obtained by simply incubating the

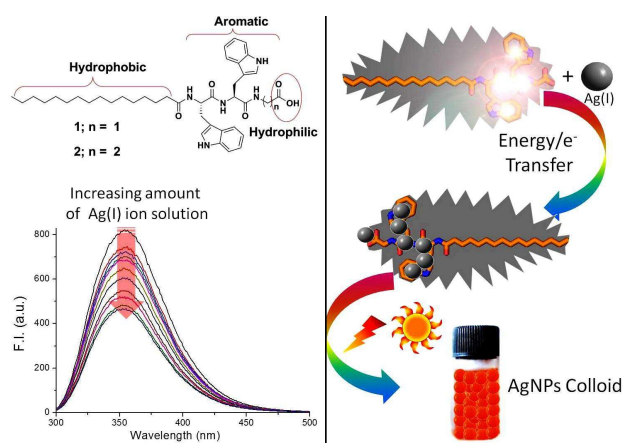


Figure 1. Fluorescence quenching of sPA **1** and **2** (10^{-5} M) by AgNO_3 solution in methanol/water (1:1). The concentration of Ag(I) was in the range of (0.5 mM – 5.0 mM). Fluorescence intensity measured at $E_{em} = 358$ nm, after excitation at $E_{ex} = 280$ nm and corresponding possible mechanism of fluorescence quenching of **1** and **2** by AgNPs.

solution of these peptide conjugates and respective metal salt followed by a short exposure to sunlight. The loading density of

^a Department of Chemistry Indian Institute of Technology Kanpur, 208016, India

^b * Dr Harisingh Gour Central University Sagar, MP, 470003, India. E-mail:

kbjoshi@dhsu.ac.in; kbjoshi77@gmail.com.

Both the authors contributed equally.

[†] Electronic Supplementary Information (ESI) available: [details of any supplementary information available should be included here]. See DOI: 10.1039/x0xx00000x

in situ synthesized nanoparticles was also controlled by changing the parameters such as pH⁴⁸, temperature⁴⁹ and solvents.⁵⁰ These hybrids showed great potential for the various biomedical applications and hence can act as theranostic agents.

Silver nanoparticles, have attracted great attention of Chemists, Physicists and Biologists owing to their interesting optoelectronic and bio-medicinal properties.⁵¹⁻⁵³ They have also been studied as biomarkers and sensors^{54,55} and are most extensively used NPs in the range of products and processes due to their wide range of biological properties and relatively low manufacturing cost.⁵⁶⁻⁵⁸ They have a broad range of applications in industries and consumer goods such as medical devices, fabrics, drinking water filters, food sprays, toys, containers, and electrical goods.⁵⁹⁻⁶² Silver nanoparticles have also been used as matrix for the laser desorption ionization mass spectrometry of peptides.⁶³ However some scientists have also studied the behaviour of AgNPs in the environment and their effects on aquatic and sedimentary organisms.⁶⁴⁻⁶⁷

Based on our growing interest in peptide self assembly and its possible application⁴⁰⁻⁴⁷, recently we have reported the defined nanostructures of tryptophan-based short peptide amphiphiles (sPA) **1** and **2** (Fig. 1).⁴⁷ The self assembled structures of these conjugates worked as a template for the synthesis of AuNPs in the presence of sunlight and during this process the morphological transition from fiber to vesicles were also observed first time.^{47, 68} Therefore the compound **1** and **2** are of particular interest and can also be used for nanofabrication of other biologically relevant metal nanoparticles for bionanotechnology application. In the milieu of above findings and inspiration from our previous work,⁴⁷ we are interested to synthesize AgNPs with the help of **1** and **2** which reduces the Ag(I) ions to Ag(0) at pH 7.0 in the presence of sunlight and worked as capping/stabilizing agents for AgNPs (Fig. 1; Right). During this process the formed AgNPs were decorated along

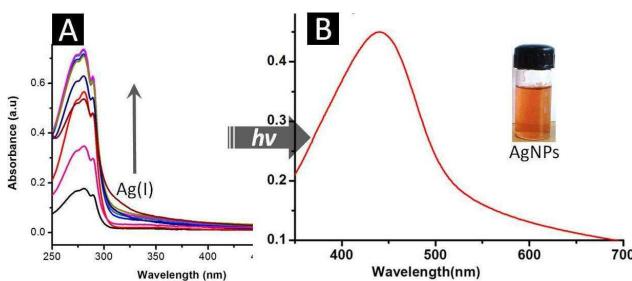


Figure 2. UV-Vis spectra of conjugate **2** in the (A) presence of increasing Ag(I) ions (1.0 mM – 6.0 mM) depicts the interaction and complex formation mainly between Trp (λ_{obs} 280 nm) side chain and Ag(I). (B) After the complex formation followed by brief exposure of sunlight formation of AgNPs were seen which were further confirmed by corresponding (B) SPR bands.

the fibrous network of sPA **1** and **2**. Such kind of synthesis and biofabrication of AgNPs with sPA is of great interest owing to their biocompatibility and ease of functionality.

Intrinsic fluorescence nature of tryptophan is well known property among other biological molecules which can be used for biomolecular recognitions and have great advantage in

biology.⁶⁹⁻⁷¹ Since sPA **1** and **2** has ditryptophan residues in its hydrophobic core therefore we started to check the interaction of **1** and **2** with Ag(I) ions with the help of fluorescence titration measurements. Interestingly we found that upon increasing concentration of Ag(I) ions to the solution of sPA, quench the Trp fluorescence several folds lower as compared to neat sPA solution, perhaps due to the FRET effect or e^- transfer mechanism from Trp residue to Ag(I) ions, clearly reveals that Ag(I) ions interact with sPA and the probable site of interaction is Trp-Trp residue (Fig. 1). This observation was further confirmed by UV-Vis titration experiments where the absorption at 280 nm was enhanced upon the addition of the increasing concentration of Ag(I) ion solution (Fig. 2 and ESI). As our previous report illustrated that brief exposure of sunlight will lead to the gold nanoparticles formation.⁴⁷ Therefore we wish to check the effect of sunlight in the sPA-Ag(I) complex solution and surprisingly we also found that upon exposure of sunlight the solution turns into yellowish orange color. The colour change is in accordance with the plasmonic characteristic of silver nanoparticles confirmed by SPR band which is centred between 400-500 nm reveals the formation of AgNPs (Fig. 2B and ESI) and supported by proposed mechanism (Fig. 1).

In our previous reports we found that the sunlight mediated reductions of Au(III) ions by sPA usually carried out by free radical mechanism⁴⁷ therefore to investigate whether photochemical reduction of Ag(I) ions by sPA would also occur in the presence of TEMPO, a free radical quenching agent. Indeed, in the presence of TEMPO we have not observed any color change in the solution, suggesting the involvement of free radical during this reduction process. Mixture of AgNO₃ solution and sPA have at pH 7.0 set aside for 1h at three different temperatures (45, 55 and 60°C) and also we did not observe any changes in the color of reaction mixture which further confirms the crucial role of sunlight in the formation of AgNPs.

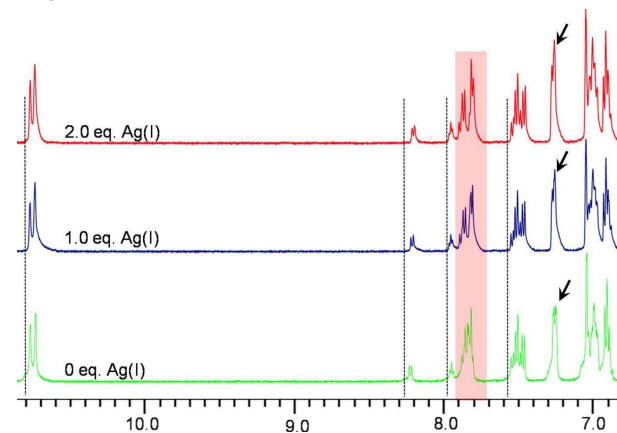


Figure 3. ¹H NMR titration spectra of sPA **2** in DMSO-*d*₆ in the presence of increasing amount of AgNO₃ solution.

To check the structural changes in sPA **1** and **2** in the presence of AgNPs we have recorded ¹H NMR spectra after the addition of Ag(I) ions in DMSO-*d*₆. The compounds were dissolved in DMSO-*d*₆ and mixed with the aqueous solution of AgNO₃ and the NMR tubes were set aside for 10-15 minute in

sunlight. We have observed the changes in aromatic protons signals after incremental addition of Ag(I) ion solution (highlighted in Fig. 3). Our observation reveals that during this process the Trp-Trp group interacts more efficiently therefore we are only interested to check the aromatic region in ^1H NMR spectra (Fig. 3 and ESI). The peak at 10.7 ppm (doublet) corresponds to the indolic protons and the multiplet peaks between 6.9-8.3 ppm corresponds aromatic and amide-protons in the molecule. The comparison with the NMR spectrum (green trace) of neat sPA and the NMR spectra after the addition of Ag(I) ions in the compound showed few extra signals in aromatic protons and slightly up field shift of other key protons were observed. This observation supports that sPA also undergoes changes during the interaction and reduction of Ag(I) ions and perhaps few oxidised products also formed during this process.

The synthesis of nanoparticles of controlled size and shape with the help of small peptides is highly demanded. We wish to check the effects of these nanoparticles on the molecular and supramolecular ensembles by spectroscopic and microscopic techniques. We have previously reported that the observed quenching attributed to an electrostatic interaction between metal ions and sPA which leads to energy transfer from Trp residue to metal ions.^{46,47} It is clear that the designed molecule(s) contain long chain fatty acid and ditryptophan as a strong hydrophobic group in the middle region however the terminal group has the little variation (Fig. 1) and it is more hydrophilic in nature compare to former two. Such special

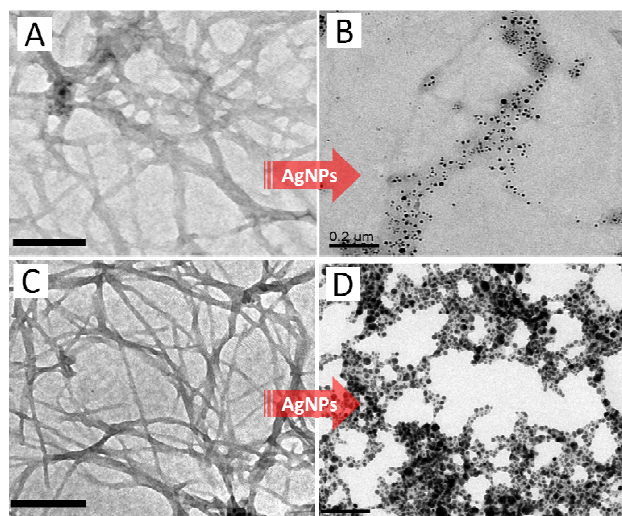


Figure 4. (A, C) TEM micrographs of **1** and **2** respectively before addition of AgNO_3 and (B, D) corresponding TEM micrographs after addition of AgNO_3 followed by 10-15 min sunlight exposure and showing the formation and decoration of AgNPs along the sPA's fiber network. Scale bar 200 nm

class of design allowed us to check the self assembly in the presence and absence of both aqueous and non aqueous media. sPA **1** and **2** are well known to rapidly self assemble into fibers which is confirm by TEM micrographs (Fig. 4). Upon addition of AgNO_3 solution followed by 10-15 minute sunlight

exposure TEM observations reveal that formation of homogeneously decorated AgNPs along the fibrous network of **1** and **2** (Fig. 4B and C). Observations also reveal that the AgNPs started to aggregate along the nanofibers of **1** and confirms that the morphology of fibers was intact during AgNPs formation. When concentrations of both Ag(I) ions and **1** were increased, the entangled and stacking nature between layers of fibers were noticed and more numbers of nanoparticles were attached to the nanofibers leading to a fibrous network decorated by AgNPs, were obtained (Fig. 4B and D). The TEM micrograph of sPA with AgNPs showed that the sophisticated hybrid structures of AgNPs-sPA were immobilized over the nanofiber, which functioned as a template and perhaps driving the nanoparticles to assemble along the nanofibers. Further we wish to check the sizes of synthesized AgNPs on the template of sPA **1** and **2** and found the sizes of nanoparticles were slightly different in each case. The particles size distribution (PSD) studies and subsequently Gaussian fitting reveals that silver nanoparticles attained maximum size in the range of 11-14 nm with the fibrous network of **1** and 15-20 nm with **2** (Fig. 5). PSD also revealed that the sPA **2** produced well defined nanoparticles as compared to sPA **1**. The particle size distribution analysis also well corresponds with SPR bands of sPA **1** and **2**.

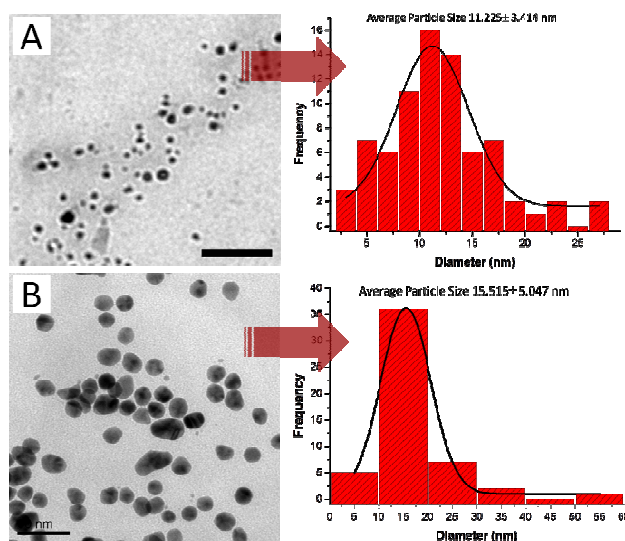


Figure 5. Particle size distribution of compound **1** and **2** conjugated with AgNPs in 50% methanol-water.

To achieve the precise deposition of AgNPs on the sPA fibers we have now taken sPA **2** as a representative molecule. The dilute solution of AgNO_3 (0.1 mM) was added to the 1 mM solution of sPA **2** followed by the brief exposure of the sunlight. The solution turn into light orange color and 1 μL aliquots of this solution was transferred onto carbon coated grid and the sample was analyzed by TEM. Interestingly we have found the precise deposition of AgNPs along the single fiber of sPA (Fig. 6A and B). Further the TEM analysis showed that monodispersed distorted spherical particles along the fiber axis (Fig. 6B and C). The selected area diffraction patterns (SADPs) illustrate the number of strong Bragg reflections which

corresponds to the (111), (200), (220) and (311) and reflections of FCC silver⁷²⁻⁷⁴ (Fig. 6D). The diffractions pattern also reveals the absence of spurious diffractions owing to other crystallographic impurities.

The high-resolution micrograph distinctly showed the lattice fringes where d , the distance between two lattice fringes, is 0.27 nm (Fig. 6E and F) typically observed for the crystallinity of AgNPs. This experiment suggests that the controlled deposition of AgNPs over the fiber of sPA and the crystalline nature of the AgNPs can lead to the useful nanodevices which could show the potential application in biomedical and nanotechnological field. Further the less or non-toxic concentration of metal nanoparticles such as silver owing to their plasmonic nature is also useful for imaging and developing bionanoprobes. The photodynamic properties of silver nanoparticles can be useful for imaging and targeted tumour destruction without damaging the surrounding healthy tissues thus, can be used for nanoparticle based theranostic agents.

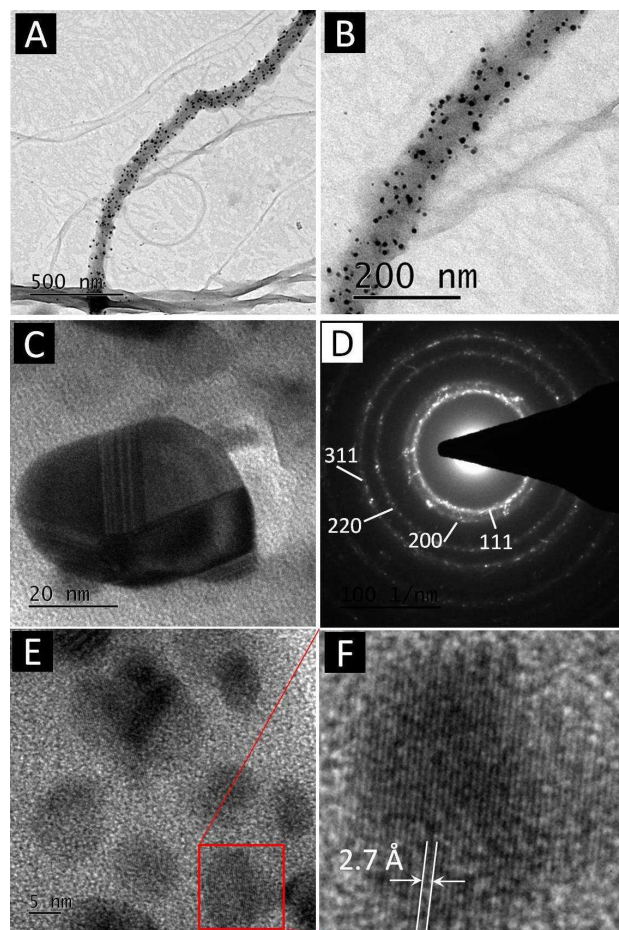


Figure 6. TEM image depicts (A and B) precise deposition of silver nanoparticles over the sPA fiber, (C) showing the distorted spherical silver nanoparticles, (D) Selected area diffraction patterns (SADPs), of silver nanoparticles confirmed the crystallinity and reflections are correspond to FCC crystal structure of silver, which is further supported by high-resolution TEM images (E and F) which distinctly

showed the lattice fringes ($d = 0.27$ nm) of AgNPs.

The conformational changes in **1** and **2** in the presence and absence of AgNPs were determined by circular dichroism (CD) study.⁷⁵ The peptide containing indolic side chain has typical CD spectrum^{46,76,77} which can show little deviation in ellipticity values due to the changes in conformation of peptide and other physical parameters. The CD spectra of sPA **1** and **2** show two extremum bands at 233 nm, 210 nm at far UV-region, and one negative extremum band at 225 nm (Fig. 7). Conformational changes were observed in the presence of AgNPs owing to the changes in the conformational state of sPA near the boundary surface of nanoparticles. CD spectra reveal that the variations in conformational changes after the conjugation of AgNPs with sPA help to determine the properties of biomolecule as well as optical and electrical properties of nanoparticles for biotechnological applications.

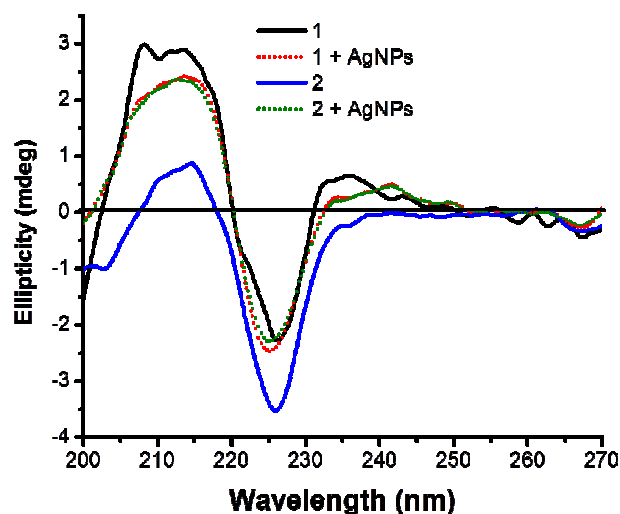


Figure 7. CD spectra of compound **1** and **2** conjugated with AgNPs in 50% methanol-water.

To understand the formations of AgNPs embedded sPA fiber, a schematic proposed mechanistic model depicts the formation of fibrous morphology which upon addition of AgNO₃ followed by sunlight irradiation showed decoration of AgNPs along with fibrous network⁷⁸ (ESI). The designed sPA molecules, typically consists of key structural features namely the long alkyl tail as a hydrophobic domain, a short aromatic dipeptide sequence capable of forming hydrophobic π - π interaction and linear amino acids which can fit into both hydrophilic or hydrophobic environments due to its minimal side chain effect and for the design of water-responsive nanostructures. It can be predicted that the hydrophobic alkyl tail specifically presents inside (ESI) the self-assembled nanostructures in aqueous methanol and enables the engineering of micelles like networks. The aromatic dipeptide sequence adjacent to the hydrophobic segment have propensity to form intermolecular hydrophobic π - π interactions and capable to stabilize these interaction and

promotes the fabrication of the unique 1D self-assembled nanostructures. The selection of linear amino acids such as Gly and β -Ala which is known for their trivial hydrophilicity incorporated into the design immediately after the aromatic peptide sequence in such a way that it should not interfere with the self-assembly of sPA but will simply increase the non covalent interactions and will further help to entangle into 3D networks followed by stabilization of 3D nanostructures. The self assembly of AgNPs-sPA arises mainly from three major energy contributions; electrostatic interactions, hydrophobic π - π interactions and hydrogen bonding. Hence a delicate balance of each of these energy contributions will finally lead to AgNPs embedded nanofibrillar assemblies (Fig. S3).

Next to check the stability of these sPA-AgNPs hybrids we have performed the thermogravimetric analysis.⁷⁹⁻⁸¹ The TGA thermogram of sPA **1** and **2** in the presence of AgNPs showed \sim 2-15% weight loss between room temperature and \sim 280 °C (ESI). This may be attributed to the loss of methanol and water from the confines of soft fibrous structures. The TGA thermogram of the sPA **1**-AgNPs hybrids initially showed a certain amount of weight decrease above 50 °C (ESI), presumably from the evaporation of water/methanol molecules that interact with the lumen of sPA **1**-AgNPs hybrids. A major decrease in weight was observed only above 290 °C for sPA **1**-AgNPs and 300 °C for sPA **2**-AgNPs due to the degradation of sPA fibers only. However the further weight loss of the sPA1-AgNPs and sPA 2-AgNPs peptide hybrids was observed at 330 °C and 345 °C respectively (ESI) and it is due to the detachment of AgNPs followed by degradation of hybrids. The derivative thermogram clearly demonstrated a similar degradation pattern, but showed sPA 2-AgNPs hybrids were more stable as compared to sPA 1-AgNPs.

To find out any changes of mechanical properties before and after AgNPs formation, we also performed rheological experiments. Interestingly we observed some changes in the mechanical properties of sPA-AgNPs hybrids and sPA alone by rheological

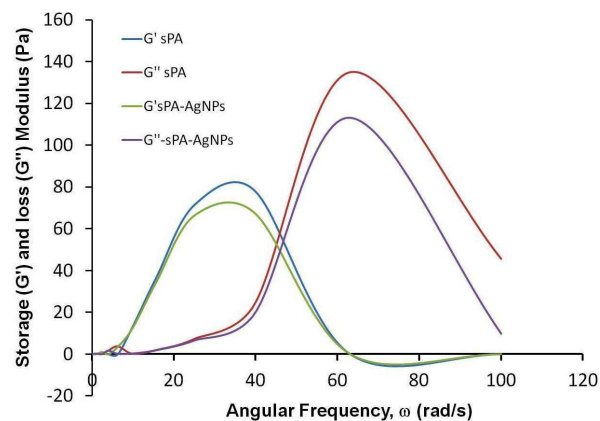


Figure 8. Depicts that the higher values (Pa) for the sPA as compare to sPA-AgNPs. The decreased value of storage and loss moduli for the sPA-AgNPs hybrids compare to the sPA alone suggesting that the silver nanoparticles are interfering and weakening the non covalent interactions between the molecules(units) of sPA hence reduce the stability of sPA fibrous network.

measurements⁸²⁻⁸⁴ (Fig. 8 and ESI). The rheological study suggested that the values of storage modulus at lower frequencies for sPA-AgNPs decreases. This decreased value of storage modulus for the sPA-AgNPs hybrids as compared to the sPA alone is perhaps due to the AgNPs are interfering and weakening the non covalent interactions between the units of sPA hence reduce the stability of sPA fibrous network. This observation corresponded well with the concentration dependent TEM observations (ESI) where the destruction of fibrous network in the presence of high concentration of Ag(I) clearly seen (ESI). Also at higher frequencies the higher values of G'' as compared to G' suggested about the viscous liquid like properties of sPA and sPA-AgNPs hybrids (ESI). The mechanical strength of sPA-AgNPs hybrids is less but more stable than sPA alone. This can be further confirmed from the graph between angular frequency, ω and the storage (G') and loss (G'') moduli where the storage and loss moduli of sPA-AgNPs hybrids are less as compared to moduli of sPA alone (Fig. 8).

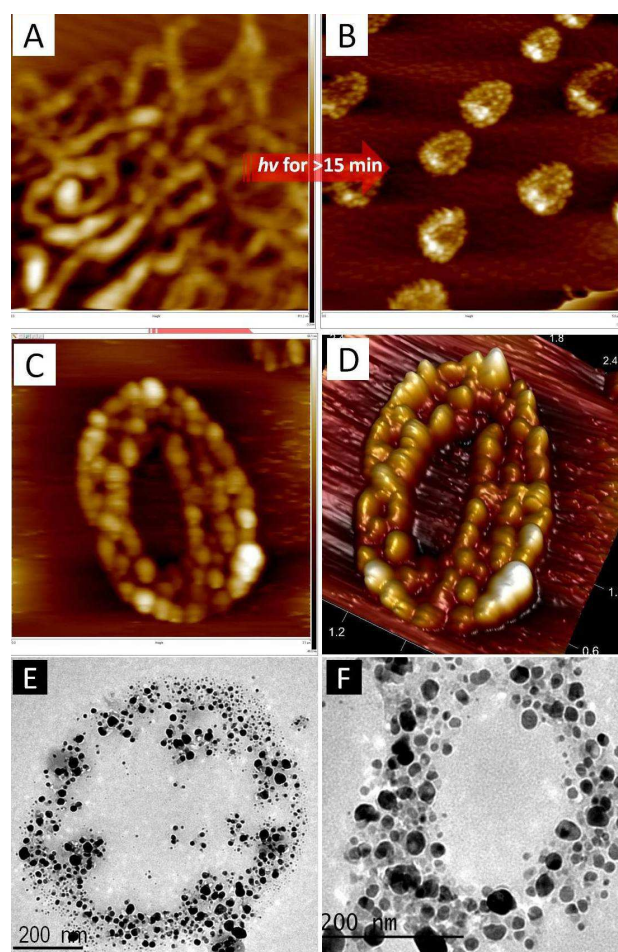


Figure 9. TOP: AFM Images of sPA-AgNPs hybrids depict effect of plasmonic heating. The sPA-AgNPs hybrids fibers are transforming their shape into nanowreath. Bottom: TEM micrograph also depicts the self-coiling of AgNPs loaded fibers during this plasmonic heating process without the use of any template or other additives which resulted in the formation of nanowreath or loop kind structures.

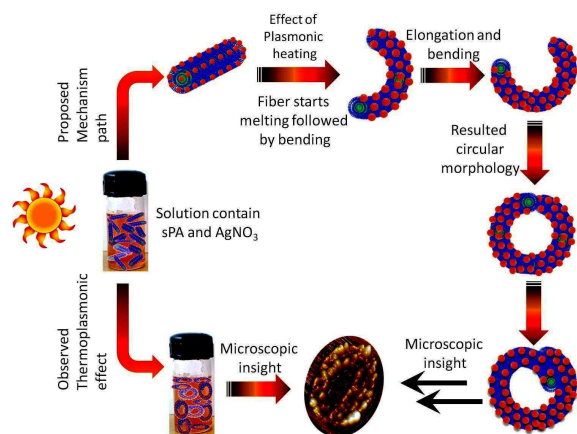


Figure 10. Plasmonic heating based shape transformation of linear fibrous structure to circular fiber structure.

Although our experimental observations reveal that sPA-AgNPs conjugates have less mechanical strength but they are more stable as compared to sPA alone, supported by TGA analysis and therefore can play vital role in several biotechnological applications. In our previous reported work we have shown the effect of plasmonic heating of AuNPs on AuNPs-peptide hybrids, therefore we are curious to know the effect of plasmonic heating on these hybrids too. It is now clear that during the formation of AgNPs, silver nanoparticles are embedded along the sPA fiber which is confirmed by TEM observations. As our objective was to check the effect of plasmonic heating on these hybrid structures; we have set aside the AgNPs-sPA solution more than 15 min (which was the sufficient time for the AgNPs preparation) under sunlight. This exposed solution was then examined under the atomic force microscope. The aliquots of over exposed solution were transferred over the freshly cleaved mica surfaces and images were taken under AFM. We assumed that the effect of heating will be more for the AgNPs-sPA compared to normal sPA fibers.

Interestingly we found that interconnected fibrous morphology of AgNPs-sPA hybrids were converted into circular form and looks like nanowreath⁸⁵ kind of assembly. Due to thermal effect of sunlight suggesting that the sPA molecules are dehydrated at the point where AgNPs are attached and their structure is broken/mould from this specific point, to form a more stable molecular unit hence lead stable nanowreath kind of morphology (Fig. 9C and D). These observations are well corresponded with TEM results (Fig. 9E and F). From this observation we have introduced a model based on AgNPs photocatalyzed effect on sPA-AgNPs hybrids (Fig. 10). Subsequently, hydrophobic forces may also drive the self-assembly into unique circularly arranged form (Fig. 10).

These results are significant because they demonstrate that short peptide amphiphile can be used to template the self-assembly of hierarchical networks of inorganic materials. More broadly, the technique used here represents a simple and eco-effective route to control the soft structure by directly

using sunlight. Based on the proposed mechanism (Fig. 9), now we wish to check the time dependent effect of sunlight on these sPA-AgNPs hybrids using AFM as powerful technique. As mentioned in our previous report the sPA 1 and 2 are well

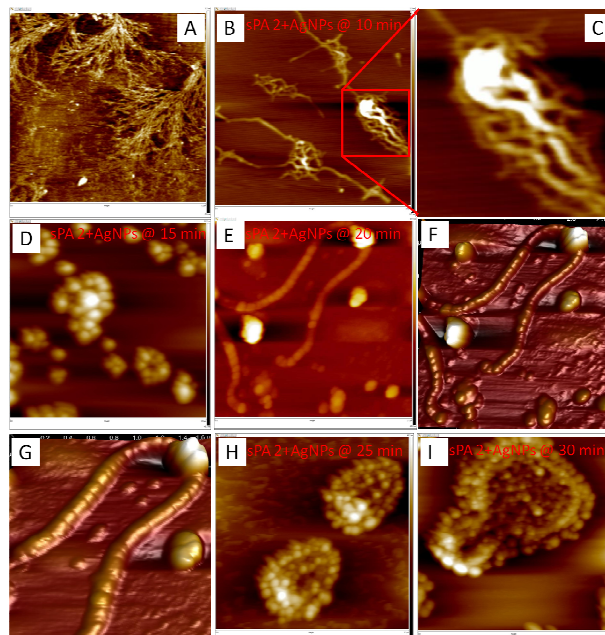


Figure 11. Time dependent AFM investigation of transforming fiber into nanowreath in the presence of sunlight. (A) Micrograph clearly depicts fibrous morphology of sPA in aqueous methanol solution, (B) the amphiphilic fiber intertwined during the formation of silver nanoparticles, (C) which can be clearly seen in a zoomed view, (D) after 10 min exposure of sunlight perhaps these structures began to organize and (E) the precise and uniform organizations of these aggregates lead to a string of beads kind of morphology (F and G) after 15 min. Upon 20 min of exposure the bead string get converted into nanowreath kind of self-assembly (H). The micrograph (I) shows that it also possible that the two or more nanowreaths can blend gradually lead to large nanowreath upon prolonged exposure.

known to form fiber in aqueous methanol which is confirmed by TEM (Fig. 4A and C). We have found the dense fibrillar structure under atomic force microscope (Fig. 11A), which get intertwined during the formation of silver nanoparticles and converted into entangled network kind of morphology (Fig. 11B and C). Further for 15 minute exposure of sunlight these entangled structure converted into random aggregates followed by the nucleation and started to organize into small circle (Fig. 11D). We assumed that this phase where the pre-organization of aggregates were seen is a nucleation phase for next step in which the energy of the system is maximum and therefore not the stable and final saturated state can be achieved. When we exposed the same solution for another 20 minute, interestingly we found that all the aggregates which we have seen in previous steps, uniformly organised which lead to a string of beads kind of morphology (Fig. 11E). The uniform organizations of aggregates were clearly visible and

can be seen in 3D AFM micrographs (Fig. 11F and G). Upon 25 min of sunlight exposure the string of uniform aggregates gets converted into nanowreath kind of structures (Fig. 11H). We have also found that two or more nanowreaths can blend gradually and lead to larger nanowreath upon prolonged exposure (Fig. 11 I).

At this stage to get more insight into these thermoplasmonic based morphological transformation from normal fiber to nanowreath like assembly we have used TEM technique. Interestingly time dependent TEM observation also reveals transition from fiber to nanowreath and corresponded well with AFM observations. The formation of silver nanoparticles started at 10 min exposure of sunlight and finally upon 15-20 min these hybrid structures get converted into nanowreaths (Fig. 12) and during this process the AgNPs were embedded along the sPA fiber in circular manner.

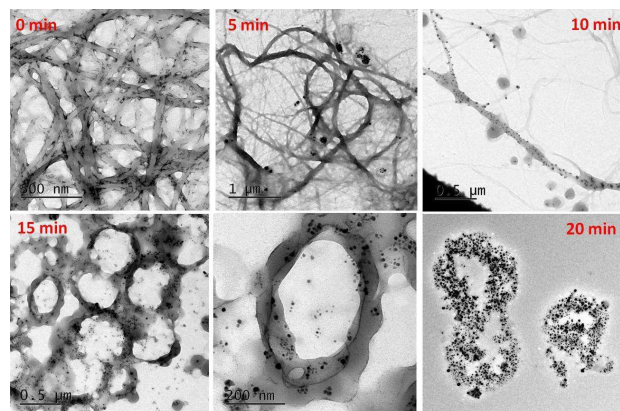


Figure 12. Time dependent TEM investigation of transforming fiber into nanowreath in the presence of sunlight after 20 min exposure of sunlight.

In order to interpret the obtained metal-hybrid based nanowreath kind of assembly obtained by TEM we have further used one common single image analysis technique that is suggested in the Matlab®.⁸⁶⁻⁸⁹ In a nanowreath the AgNPs are embedded to sPA fiber, resulted in nanowreath morphology, which was obtained by thermoplasmonic effect of AgNPs. To check whether the obtained metal-hybrid based morphology was due to the above said effect or just due the organization of AgNPs only,⁶⁸ we have processed this image with image processing tool box in Matlab (Fig. 13). Our observation reveals that after the processing of image the nanoparticles embedded fiber was clearly visible (Fig. 13B) which was not visible before processing (Fig. 13A). In the final processed image only fiber was clearly observed after the complete subtraction of background and nanoparticles (Fig. 13C). This observation further confirmed that the nanoparticles are embedded over the fibrous morphology and moulded into circular shape due to thermoplasmonic effect of nanoparticles. Further the presence of moulded fiber can be confirmed through covariance matrix, a statistical analysis, of images shown in Fig. 13 (bottom). Images in Fig. 13, reveal the plot of covariance matrix for unprocessed, intermediate and

final processed TEM images respectively. Covariance matrix confirmed the correlation between the elements present at the pixels in images. The large value of covariance implies a strong correlation while smaller one shows a weak correlation. It can be observed in Fig. 13 that the correlation is in increasing order as we move from Fig. 13A' to Fig. 13C'. Further, in the figure the value of covariance is shown by colors. The blue color represents the smallest one while red shows the largest one. It can be seen that the presence of green color is increasing nearby the diagonal which confirms the larger

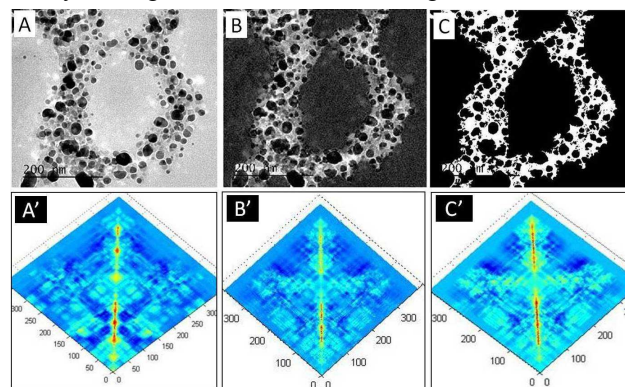


Figure 13. Processed TEM image by image processing tool box in Matlab. **Top:** (A) depicts the TEM image which is a combination of fiber and nanoparticles where fiber is not visible, (B) Intermediate processed image, subtraction of background only, fiber is visible now and (C) final processed image; subtraction of background and nanoparticles both, clearly depict the fiber was moulded by thermoplasmonic effect of nanoparticles. **Bottom:** corresponding covariance matrix plot of (A-A') unprocessed image, (B-B') intermediate processed image and (C-C') final processed Image. Covariance matrix shows the correlation between the elements present at the pixels in images, the blue color represents the smallest one while red shows the largest one.

correlation between the objects present at that location in corresponding image. The larger value of covariance showed the presence of single type of species in the image, since similar objects have strong correlation than different types of objects. Hence increasing order of correlation reflects the presence of one kind of object in the final processed image in (Fig. 13C'). Further Fig. 13A' the covariance has smaller values, which showed the presence of both fiber and nano particle as there is no correlation between the morphology of these objects. In addition to this Fig. 13B' reflects the covariance has large and small both type of values at various locations, which confirmed that image processing tool has improved the locations of strongly correlated and weakly correlated objects in intermediate processed image. They are independent objects hence they must reflect in the TEM images independently as shown in Fig. 13B'.

In another control experiment, the pre-synthesized AgNPs (15–20 nm) using sodium citrate method, were mixed with sPA 2 (1 mM, 50% aqueous–methanol). TEM micrographs revealed that the fibrous morphology accumulated and get converted into

a discrete fractal-kind of structures which also support the probable role of AgNPs in self-assembly (Fig. 13).

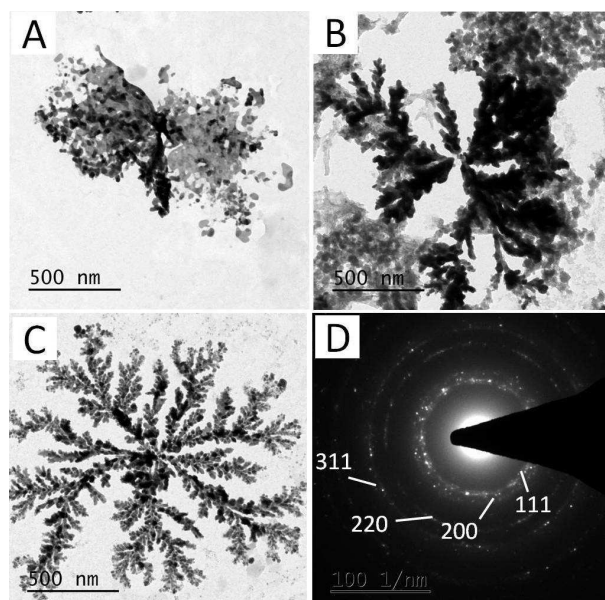


Figure 13: Depicts the role of presynthesized AgNPs. (A) TEM image after the addition of presynthesized AgNPs at 0 min, (B) after 5 min and (C) after 10 min shows fractal kind of morphology. Micrograph (D) also reveals that fcc nature of AgNPs.

Conclusions

Thus, we have demonstrated a simple technique for the synthesis of AgNPs with the help of small peptide amphiphiles in the presence of sunlight. The AgNPs were homogeneously decorated along the fibrous network which serve as a scaffold and investigated by various spectroscopic and microscopic techniques. Interestingly our results highlight these AgNPs embedded sPA fibers were moulded by simple plasmonic heating based experiments and resulted in circularly arranged morphology which resembles with nanowreath.^[84] To the best of our knowledge and literature survey such kind of metal-hybrid structure were observed first time. The thermoplasmonic effect of biologically relevant metal showed great importance to mould/bend the peptide based soft nanostructures and can be used for several biomedical applications⁹⁰ such as diagnostic agents and treatments of various ailments, hence can work as theranostic agents too. These reported results could be of great interest owing to the thermoplasmonic effect of silver nanoparticles which transform the short peptide amphiphile fiber to AgNPs garlanded nanowreath assembly,⁹¹ a unique peptide-metal based assembly and can show the potential application in the field of nanotechnology.

Experimental section

General- Methanol, Water, AgNO₃ were purchased from Spectrochem, Mumbai, India, and used without further purification.

Atomic Force Microscopy (AFM) – Neat and co-incubated solution of sPA with AgNPs was imaged with an atomic force microscope. The samples were placed on freshly cleaved muscovite mica surfaces followed by imaging with an atomic force microscope (INNOVA, ICON analytical equipment, Bruker, Sophisticated Instrument Center (SIC)-Dr. Harisingh Gour Central University, Sagar-M.P.) operating under the acoustic AC mode (AAC or tapping mode), with the aid of a cantilever (NSC 12(c) from MikroMasch, Silicon Nitride Tip) by NanoDrive™ version 8 software. The force constant was 2.0 N/m, while the resonant frequency was ~290 kHz. The images were taken in air at room temperature, with the scan speed of 1.5-2.0 lines/sec. The data analysis was done using of nanoscope analysis software. The sample-coated substrates were dried at dust free space under 60W lamp for 6h followed by high vacuum drying and subsequently examined under AFM.

Transmission Electron Microscopy (TEM) – The samples were placed on a 400 mesh carbon coated copper grid. After 1 minute, excess fluid was removed and the grid was/wasn't negatively stained with 2% uranyl acetate solution. Excess stain was removed from the grid and the samples were viewed using a FEI Technai 20 U Twin Transmission Electron Microscope, operating at 80 kV. The microscope is a STEM and is also equipped with a EDS detector, HAADF detector and Gatan digital imaging system.

Fluorescence studies- Fluorescence spectra were recorded on varian luminescence cary eclipsed and CARY win 100 Bio UV-Vis spectrophotometer with a 10 mm quartz cell at 25 ± 0.1 °C. The solutions of sPA and Ag(I) salt were prepared separately in CH₃OH/H₂O (50:50). Deionized water and methanol (HPLC grade) were used in these studies. The solution containing sPA (10⁻⁵ M) and different concentrations of silver salt in different ratios were prepared and recorded their fluorescence spectra in fresh as well as in aged conditions. All fluorescence scans were saved as ACSII files and further processed in Excel™ to produce all graphs shown.

Circular Dichroism spectroscopy- All CD experimnt were carried out at room temperature. Spectra were collected at final concentration for each at 100 μM of sPA **1** and **2** alone and with in situ prepared silver nanoparticle, on JASCO J-815 CD SPECTROMETER by using quartz cuvette with a path length of 1mm. CD spectra were collected between 195 nm to 270 nm and each spectrum were the average of 5 scans. To avoid any instrumental baseline drift between any measurements, the background value was substracted for each individual sample measurement with 50% methanol-water.

Preparation of AgNPs: To the freshly prepared solution of compound **1** and **2** (1mM, 1mL) in methanol water (1: 1), 50μL, AgNO₃ added from the stock solution of AgNO₃ (10⁻³ M) was added separately and the mixture was kept in sunlight for 10-15 minute. A characteristics colour of silver nanoparticle was appeared with an appropriate SPR band at ~450 nm and confirmed the formation of AgNPs.

Purification of silver nanoparticle colloid: Purification of silver nanoparticle colloid done by using centrifugation method before using it for the imaging/analysis. After the formation of AgNPs-Peptide hybrids the solution was centrifuged at 12,000g for 30 minutes followed by removal of the supernatant and washing with

methanol. The residue/pallets were re-dissolved in the 50% aqueous methanol in the appropriate volume of solvent. The colloid solution was stable for several days.

Rheometry: Rheological assays were performed on a 50 mm parallel plate Modular Compact Rheometer, MCR 502 by Anton Paar. Samples were dissolved in 50% methanol-water at a final concentration of 4 mM and sonicated for 15 minutes, one day before analysis. A volume of 3 mL of sample was loaded on the lower plate, and the upper plate was set to a gap size between 0.4 and 0.45 mm. Dynamic frequency sweep tests were performed in a range of frequencies from 100 to 0.1 rad/s. Solution of silver ions with optimum concentration was added to sPA followed by 15 min sunlight exposure. The characteristic color change of silver nanoparticles was appeared and this solution was used for the rheology.

Image Processing by MATLAB: Image background was estimated by using morphological operation function. This estimated background was subtracted from the main image. The image contrast was improved and then grayscale image was changed into binary image for further processing. The function "graythresh" was used to compute an appropriate threshold to use to convert the grayscale image to binary. Further, background noise was removed with function "bwareopen" and obtained the final processed image.

Acknowledgements

NKM and VK thank CSIR-India and NFOBC-UGC-India for pre-doctoral research fellowship respectively and contributed equally to this work. Authors thank to Prof. Sandeep Verma, IIT Kanpur for providing the research facility and his constant invaluable support to carry out the work successfully and Sophisticated Instrument Centre (SIC)-Dr. Harisingh Gour Central University Sagar-India for AFM, TEM and Rheometer facility. Our acknowledgment is incomplete without thanking Dr. Prashant Shukla (Department of Physics, Dr. Harisingh Gour Central University Sagar, M.P.) for the analysis of TEM images by MATLAB. This work is supported by UGC-BSR scheme to KBJ from University Grant Commission (UGC), India.

Notes and references

- J. Huang, L. Lin, D. Sun, H. Chen, D. Yang and Q. Li, *Chem. Soc. Rev.*, 2015, **44**, 6330-6374.
- C. L. Chen and N. L. Rosi, *Angew. Chem. Int. Ed.* 2010, **49**, 1924-1942.
- S. Banerjee, T. Maji, T. K. Paira and T. K. Mandal, *Macromol. Rapid Commun.*, 2013, **34**, 1480-1486.
- S. Roy, A. Baral and A. Banerjee, *ACS Appl. Mater. Interfaces*, 2014, **6**, 4050-4056.
- S. Cavalli, F. Albericio and A. Kros, *Chem. Soc. Rev.*, 2010, **39**, 241-263.
- S. E. Paramonov, H. W. Jun and J. D. Hartgerink, *J. Am. Chem. Soc.*, 2006, **128(22)**, 7291-7298.
- M. P. Lutolf and J. A. Hubbell, *Nature Biotech.*, 2005, **23**, 47-55.
- P. Graf, A. Manton, A. Foelske, A. Shkilnyy, A. Mas̃ic, A. F. Thunemann and A. Taubert, *Chem. Eur. J.*, 2009, **15**, 5831-5844.
- J. B. Herzog, M. W. Knight, and D. Natelson, *Nano Lett.*, 2014, **14(2)**, 499-503.
- R. Singh, P. Wagh, S. Wadhvani, S. Gaidhani, A. Kumbhar, J. Bellare and B. A. Chopade, *Int. J. Nanomed.*, 2013, **8**, 4277-4290.
- W. L. Chou, D. G. Yu and M. C. Yang, *Polym. Advan. Technol.* 2005, **16**, 600-607.
- S. Zhang, D. M. Marini, W. Hwang and S. Santoso, *Curr. Opin. Chem. Biol.* 2002, **6(6)**, 865-871.
- T. K. Paira, A. Saha, S. Banerjee, T. Das, P. Das, N. R. Jana and T. K. Mandal, *Macromol. Biosci.* 2014, **14**, 929-935.
- J. Bhaumik, N. S. Thakur, P. K. Aili, A. Ghanghoriya, A. K. Mittal and U. C. Banerjee, *ACS Biomater. Sci. Engin.*, 2015, **1(6)**, 382-392.
- Y. T. Yen, C. W. Chen, M. Fang, Y. Z. Chena, C. C. Laia, C. H. Hsua, Y. C. Wang, H. Lin, C. H. Shen, J. M. Shieh, J. C. Hob and Y. L. Chueh, *Nano Energy*, 2015, **15**, 470-478.
- A. O. Govorov and H. H. Richardson, *Nanotoday*, 2007, **2(1)**, 30-38.
- L. A. Austin, B. Kang, C. W. Yen, and M. A. El-Sayed, *Bioconjugate Chem.*, 2011, **22(11)**, 2324-2331.
- E. K. Lim, T. Kim, S. Paik, S. Haam, Y. M. Huh and K. Lee, *Chem. Review* 2015, **115(1)**, 327-394.
- L. C. Kennedy, L. R. Bickford, N. A. Lewinski, A. J. Coughlin, Y. Hu, E. S. Day, J. L. West and R. A. Drezek, *Small*, 2011, **7(2)**, 169-183.
- T. Udaya, B. Rao, B. Nataraju, and T. Pradeep *J. Am. Chem. Soc.*, 2010, **132**, 16304-16307.
- M. P. Melancon, M. Zhou and C. Li, *Acc. Chem. Res.*, 2011, **44(10)**, 947-956.
- S. Y. Shim, D. K. Lim and J. M. Nam, *Nanomedicine*, 2008, **3**, 215-232.
- S. Mukherjee, D. Chowdhury, R. Kotcherlakota, S. Patra, V. kumar B, M. P. Bhadra, B. Sreedhar and C. R. Patra, *Theranostics*, 2014, **4(3)**, 316-335.
- S. Roy, A. Baral and A. Banerjee, *Chem. Eur. J.*, 2013, **19**, 14950-14957.
- R. M. Amin, M. B. Mohamed, M. A. Ramadan, T. Verwanger and B. Krammer, *Nanomedicine* 2009, **4(6)**, 637-643.
- J. Politi, J. Spadavecchia, M. Iodice and L. de Stefano, *Analyst*, 2015, **140**, 149-155
- J. Xie and S. Jon, *Theranostics* 2012, **2(1)**, 122-124.
- V. Castelletto, I. W. Hamley, J. Adamcik, R. Mezzenga and J. Gummel, *Soft Matter*, 2012, **8**, 217-226.
- R. Chapman, M. Danial, M. Liang Koh, K. A. Jolliffe and S. Perrier, *Chem. Soc. Rev.*, 2012, **41**, 6023-6041.
- P. Duan, L. Qin, X. Zhu and M. Liu, *Chem. Eur. J.* 2011, **17**, 6389-6395.
- H. Cui, T. Muraoka, A. G. Cheetham, and S. I. Stupp, *Nano Lett.*, 2009, **9(3)**, 945-951.
- K. T. Nam, Y. J. Lee, E. M. Krauland, S. T. Kottmann and A. M. Belcher, *ACS Nano*, 2008, **2(7)**, 1480-1486.
- C. Jo Carter, C. J. Ackerson and D. L. Feldheim, *ACS Nano*, 2010, **4(7)**, 3883-3888.
- A. M. Schrand, L. K. Braydich-Stolle, J. J. Schlager, L. Dai and S. M. Hussain, *Nanotechnology*, 2008, **19**, 235104-235117.
- R. Lévy, N. T. K. Thanh, R. C. Doty, I. Hussain, R. J. Nichols, D. J. Schiffrin, M. Brust and D. G. Fernig, *J. Am. Chem. Soc.*, 2004, **126(32)**, 10076-10084.
- V. M. Yuwono and J. D. Hartgerink, *Langmuir*, 2007, **23(9)**, 5033-5038.
- L. A. Stearns, R. Chhabra, J. Sharma, Y. Liu, William T. Petuskey, H. Yan and J. C. Chaput, *Angew. Chemie.*, 2009, **121(45)**, 8646-8648,
- C. Guo, Y. Luo, R. Zhou and G. Wei, *ACS Nano*, 2012, **6(5)**, 3907-3918.
- M. Reches and E. Gazit, *Nano Lett.*, 2004, **4(4)**, 581-585.
- C. Ménard-Moyon, V. Venkatesh, K. V. Krishna, F. Bonachera, S. Verma and A. Bianco, *Chem. Eur. J.* 2015, **21(33)**, 11681-11686.

41. S Ghosh, M. Reches, Gazit E and S. Verma, *Angew. Chem., Int. Ed.* 2007, **46**, 2002-2004
42. S. Ghosh, S. K. Singh and S. Verma, *Chem. Commun.*, 2007, 2296-2298.
43. K. B. Joshi and S. Verma, *Angew. Chem. Int. Ed.* 2008, **47**, 2860-2863.
44. K. B. Joshi, P. Singh and S. Verma, *Biofabrication* 2009, **1**, 025002.
45. A. K. Barman and S. Verma, *Chem. Commun.* 2010, **46**, 6992-6994.
46. N. K. Mishra, V. Kumar and K. B. Joshi, *RSC Adv.*, 2015, **5**, 64387-64394.
47. N. K. Mishra, K. B. Joshi and S. Verma, *J. Colloid Interface Sci.*, 2015, **455**, 145-153.
48. M. Wuithschick, B. Paul, R. Bienert, A. Sarfraz, U. Vainio, M. Sztucki, R. Kraehnert, P. Strasser, K. Rademann, F. Emmerling, and J. Polte, *Chem. Mater.*, 2013, **25(23)**, 4679-4689.
49. S. Magdassi, M. Grouchko, O. Berezin and A. Kamyshny, *ACS Nano*, 2010, **4(4)**, 1943-1948.
50. R. P. Bagwe and K. C. Khilar, *Langmuir*, 2000, **16(3)**, 905-910.
51. C. Lok, C. Ho, R. Chen and C. M. Che, *J. Proteome Res.*, 2006, **5**, 916-924.
52. J. R. Morones, A. Camacho, K. Holt, J. T. Ramirez and M. J. Yacamán, *Nanotechnology*, 2005, **16**, 2346-2353.
53. J. Kreuter and S. Gelperina, *Tumori.*, 2008, **94**, 271-277.
54. S. K. Gogoi, P. Gopinath, A. Paul, A. Ramesh, S. S. Ghosh and A. Chattopadhyay, *Langmuir*, 2006, **22**, 9322-9328.
55. U. Samuel and J. P. Guggenbichler, *Int. J. Antimicrob. Agents*, 2004, **23**, 75-78.
56. W. Lesniak, A. U. Bielinska, K. Sun, K. W. Janczak, X. Shi, J. R. Baker and L. P. Balogh, *Nano Lett.*, 2005, **5**, 2123-2130.
57. P. V. Asharani, Y. L. Wu, Z. Gong and S. Valiyaveetil, *Nanotechnology*, 2008, **19**, 1-8.
58. S. Ruden, K. Hilpert, M. Berditsch, P. Wadhvani and A. S. Ulrich, *Antimicrob. Agents and Chemother.*, 2009, **53(8)**, 3538-3540.
59. F. G. Rutberg, M. V. Dubina, V. A. Koliakov, F. V. Moiseenko, E. V. Ignateva, N. M. Volkov, V. N. Snetov and A. Y. Stogov, *Biochem Biophys.*, 2008, **421**, 191-193.
60. G. Holla, R. Yeluri and A. K. Munshi, *Contemp Clin. Dent.* 2012, **3**, 288-293.
61. P. Dibrov, J. Dzioba, K. K. Gosink and C. C. Ha'se, *Chemother.* 2002, **46**, 2668-2670.
62. A. Ravindran, P. Chandran and S. S. Khan, *Colloids and Surfaces B: Biointerfaces*, 2013, **105**, 342-352.
63. L. Hua, J. Chen, L. Ge and S. N. Tan, *J. Nanoparticle Res.*, 2007, **9(6)**, 1133-1138.
64. R. R. Naik, S. J. Stringer, G. Agarwal, S. E. Jones and M. O. Stone, *Nature Mat.*, 2002, **1**, 169-172.
65. W. K. Jung, H. C. Koo, K. W. Kim, S. Shin, S. H. Kim and Y. H. Park, *Appl. Env. Microbiol.* 2008, **74(7)**, 2171-2178.
66. A. M. Fayaz, K. Balaji, M. Girilal, R. Yadav, P. T. Kalaichelvan and R. Venketesan, *Nanomedicine: Nanotechnol. Biol. Med.*, 2010, **6**, 103-109.
67. C. N. Lok, C. M. Ho, R. Chen, Q. Y. He, W. Y. Yu, H. Sun, P. K. H. Tam, J. F. Chiu and C. M. Che, *J. Proteome Res.*, 2006, **5**, 916-924.
68. A. Biswas and A. Banerjee, *Soft Mat.*, 2015, **11**, 4226-4234.
69. S. Gorinstein, I. Goshev, S. Moncheva, M. Zemser, M. Weisz, A. Caspi, I. Libman, H. T. Lerner, S. Trakhtenberg, and O. M. Beloso., *J. Protein Chem.*, 2000, **19(8)**, 637-642.
70. D. Creed, *Photochem. Photobiol.*, 1984, **39(4)**, 531 - 562.
71. E. Silva, R. Ugarte, A. Andrade and A. M. Edwards, *J. Photochem. Photobiol. B: Biol.*, 1994, **23**, 43-48.
72. A. Courty, A. Mermet, P. A. Albouy, E. Duval and M. P. Pileni, *Nature Mat.* 2005, **4**, 395-398.
73. G. Li, D. He, Y. Qian, B. Guan, S. Gao, Y. Cui, K. Yokoyama and L. Wang, *Int. J. Mol. Sci.*, 2012, **13**, 466-476.
74. T. Theivasanthi and M. Alagar, *Nano Biomed. Eng.*, 2012, **4(2)**, 58-65.
75. N. M. Green, W. P. Mose and P. M. Scopes, *J. Chem. Soc. (C)*, 1970, 1330-1333.
76. S. M. Kelly and N. C. Price, *Curr. Protein Pept. Sci.*, 2000, **1**, 349-384.
77. H. E. Auer, *J. Am. Chem. Soc.*, 1973, **95**, 3003-3011.
78. P. P. Bose, M. G. B. Drew, and A. Banerjee, *Org. Lett.*, 2007, **9**, 2489-2492.
79. R. Manjumeena, D. Duraibabu, J. Sudha and P. T. Kalaichelvan, *J. Environ. Sci. and Health, Part A*, 2014, **49**, 1125-1133.
80. E. Boanini, P. Torricelli, M. C. Cassani and G. A. Gentilomi, *RSC Adv.*, 2014, **4**, 645-652.
81. H. L. Liu, S. A. Dai, K. Y. Fu and S. H. Hsu, *Int. J. Nanomedicine* 2010, **5**, 1017-1028.
82. S. Sathaye, A. Mbi, C. Sonmez, Y. Chen, D. L. Blair, J. P. Schneider and D. J. Pochan, *Nanomed Nanobiotechnol*, 2015, **7**, 34-68.
83. O. B. Ayyub and P. Kofinas, *ACS Nano*, 2015, **9(8)**, 8004-8011.
84. K. M. Hansson, P. Tengvall, I. Lundström, M. Raenby and T. L. Lindahl, *Biosensors and Bioelectronics*, 2002, **17**, 747-759.
85. P. R. Sajanlal, T. S. Sreeprasad, A. K. Samal and T. Pradeep, *Nano Reviews*, 2011, **2**, 5883-5945.
86. K. Liu, A. Lukach, K. Sugikawa, S. Chung, J. Vickery, H. T. Aubin, B. Yang, M. Rubinstein and E. Kumacheva, *Angew. Chem. Int. Ed.*, 2014, **53**, 2648-2653.
87. P. Han, A. R. Kurland, A. N. Giordano, S. U. Nanayakkara, M. M. Blake, C. M. Pochan and P. S. Weiss, *ACS Nano*, 2009, **3(10)**, 3115-3121.
88. W. S. Law, H. Chen, J. Ding, S. Yang, L. Zhu, G. Gamez, K. Ching, Y. Ren and R. Zenobi, *Angew. Chem. Int. Ed.*, 2009, **48**, 8277-8280.
89. E. Ringe, R. P. Van Duyne and L. D. Marks, *Nano Lett.*, 2011, **11**, 3399-3403.
90. H. Xu and K. S. Suslick, *ACS Nano*, 2010, **4**, 3209-3214.
91. J. Liu, X. Zhang, M. Yu, S. Li, and J. Zhang, *small*, 2012, **8(2)**, 310-316.